Geophysical Research Letters

Supporting Information for

Limited Regional Aerosol and Cloud Microphysical Changes Despite Unprecedented Decline in Nitrogen Oxide Pollution During the February 2020 COVID-19 Shutdown in China

Michael S. Diamond & Robert Wood

Department of Atmospheric Sciences, University of Washington, Seattle, USA

Contents of this file

Introduction

This file contains supporting information documenting:

Text S1: Technical details about the satellite retrievals used

Figures S1-5: Details of the equation (1) regression analysis including timeseries of the regressors (Figure S1); maps of diagnostics for each target variable (Figure S2); and intercepts and regression coefficients for $\ln(NO_2)$ (Figure S3), AOD (Figure S4), and r_e (Figure S5)

Figure S6: The timeseries of SO_2 averaged over eastern China, excluding major volcanic events

Figure S7: Probability of detection for $\ln(NO_2)$, AOD, and r_e (low and high sensitivity)

Figures S8-11: Details of the equation (5) regression analysis maps of diagnostics for each target variable (Figure S8); and intercepts and regression coefficients for $\ln(NO_2)$ (Figure S9), AOD (Figure S10), and r_e (Figure S11)

Figure S12: Timeseries of regionally-averaged results for the equation (5) regression analysis

Figure S13: Decomposition of emissions- and meteorology-related effects for February 2020

Figure S14: February 2005-2019 climatology and February 2020 meteorological anomalies

Figure S15: Timeseries of various economic indicators from 2005-2020

Figure S16: Accumulated growth rates from January-March 2020 (as compared to 2019) for each of the economic indicators shown in Figure S15

Figure S17: Maps of 2015 NO_x, $PM_{2.5}$, and SO_2 emissions from EDGAR

Figure S18-19: Timeseries of single-scatter albedo and Ångström exponent results from the equation (1) regression analysis (S18) and maps of 2015-2019 mean values and the difference between observed and expected February 2020 values (S19)

Tables S1-3: NO_x, $PM_{2.5}$, and SO_2 emissions summed over the region indicated in Figure 5 for the transportation sectors (Table S1), industry and power sectors (Table S2), and other sectors (Table S3)

Text S1.

The Dutch-Finnish Ozone Monitoring Instrument (OMI), a hyperspectral ultraviolet and visible light spectrometer, was launched as part of NASA's Aura satellite in July 2004. The unusual stability of OMI over its now-sixteen-year lifetime, as compared to other ultraviolet imagers, makes it ideal for evaluating long-term trends (Levelt et al., 2018). A "row anomaly" has corrupted data from particular fields of view, likely due to a physical blockage from outside the instrument, meaning global OMI coverage is accomplished within 2 days rather than 1 day (Krotkov et al., 2017; Levelt et al., 2018). Krotkov et al. (2016) contains a useful discussion of how the NO_2 and PBL SO_2 retrievals have evolved over the lifetime of the OMI/Aura mission, which we draw from heavily here.

In this work, we use the operational NASA product OMNO2d for NO_2, which performs very similarly to an alternative operational product produced by the Royal Netherlands Meteorological Institute. Both operational products share a Differential Optical Absorption Spectroscopy (DOAS) fitting of spectral measurements between 405-465 nm to laboratory-measured absorption spectra of NO_2, H_2O, and O_3 to estimate slant column densities of NO_2, which are then converted to tropospheric vertical column densities (VCDs) by subtracting a stratospheric contribution and accounting for factors such as viewing geometry, cloud contamination, and an a priori NO_2 vertical profile shape estimate. Relative errors in the tropospheric VCDs are ~20% for cloud-free polluted scenes. Cloud-screened (below 30%) Level 3 fields are created by screening for solar zenith angle and retrieval quality and then averaging pixels weighted by their overlap with each 0.25° by 0.25° grid box (Krotkov et al., 2019). We create monthly averages by taking a temporal average of the Level 3 daily values weighted by the provided factors, as described in equation (5) of Krotkov et al. (2019).

For planetary boundary layer SO_2, we use the operational NASA product OMSO2e, which uses a principal component analysis technique on OMI radiances between 310.5-340 nm to retrieve PBL SO_2. Relative errors are ~70-150% for a single retrieval but can be reduced by temporal averaging. We create monthly averages by taking an unweighted temporal average of all valid Level 3 daily values.

The NASA Moderate Resolution Imaging Spectroradiometer (MODIS) has 36 visible and infrared channels which can be used to retrieve a number of cloud and aerosol optical properties (Platnick et al., 2017). For aerosol optical depth at 550 nm, we use the operational combined ocean and land retrieval product (Aerosol_Optical_Depth_Land_Ocean). A minimum of 3 days of valid AOD retrievals is required to calculate a monthly mean and each valid daily AOD value is weighted equally in the monthly mean (Hubanks et al., 2019). For liquid cloud effective radius, we use the operational product (Cloud_Effective_Radius_Liquid) retrieved jointly with cloud optical depth using a bispectral method with the 2.1 μm and either the 0.66 μm (land) or 0.86 μm (ocean) channels. Monthly mean values are calculated by averaging daily values weighted by liquid cloud pixel count (Hubanks et al., 2019).

NASA's Deep Blue algorithm was designed to improve the retrieval of aerosol optical properties over land surfaces, where surface reflectance at red and near-infrared wavelengths can overwhelm the aerosol signal but surface reflectance at blue wavelengths is more limited (Hsu et al., 2013). After screening for clouds, snow, and ice, multiple channels (0.412, 0.47, 0.65, 0.86, 1.2, and 2.1 μm) are used to determine a surface reflectance value and aerosol model. A maximum likelihood method matches the measured 0.41, 0.47, and 0.65 μm reflectances to an appropriate combination of aerosol optical thickness and single-scattering albedo or Ångström exponent using lookup tables. We use the single-scatter albedo calculated at 470 nm for our analysis. A minimum of 3 days of valid retrievals of ω_0 and α is required to calculate a monthly mean (Hubanks et al., 2019).

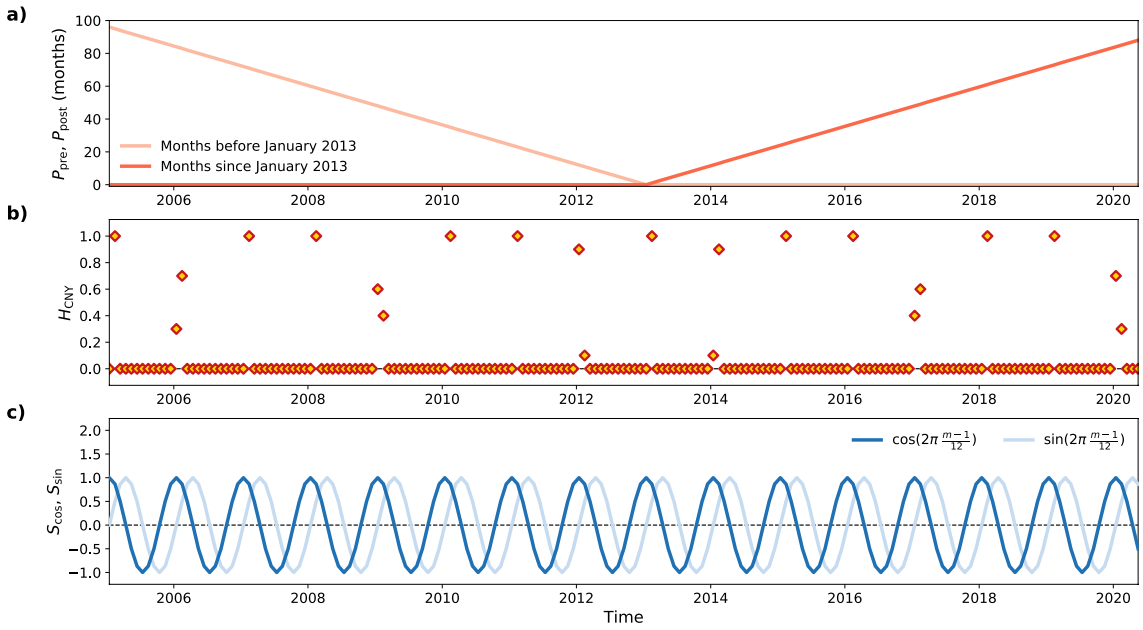

Figure S1. Time series of regressors for the model described by equation (1). **a)** Trends for the time period before (P_{pre}) and after (P_{post}) January 2013, the policy "turning point" after which stricter clean air rules were put into effect. **b)** Holiday effect H_{CNY} defined as full or partial occurrence of Chinese New Year festivities in a given month. **c)** Idealized seasonal cycles S_{cos} and S_{sin}.

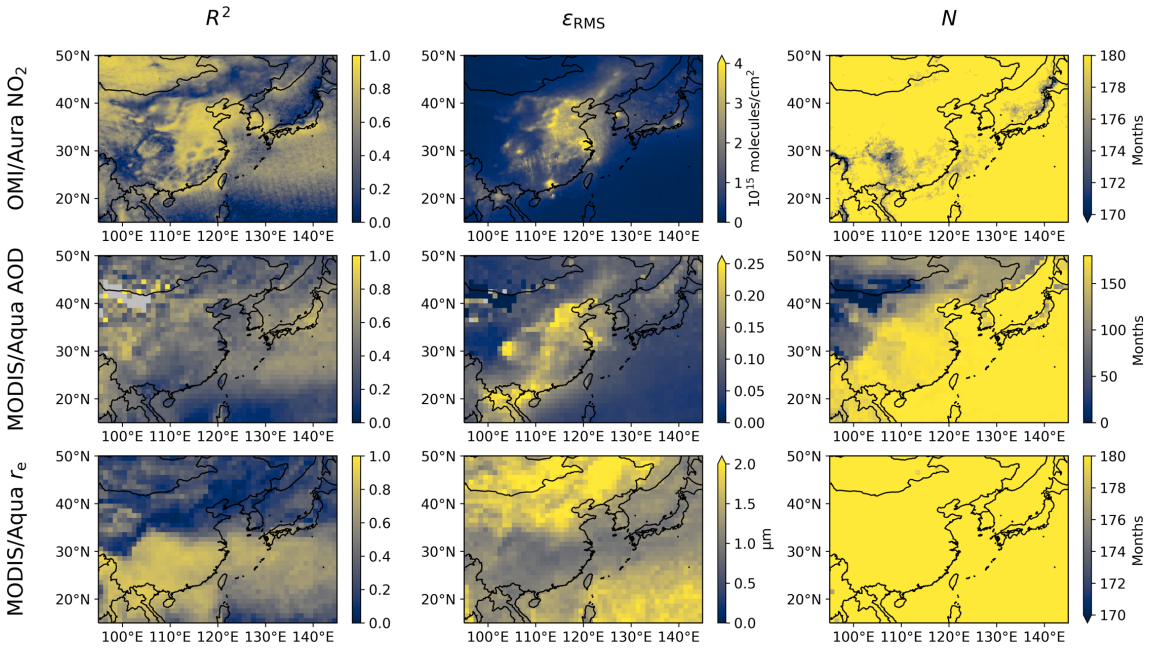

Figure S2. Maps of regression diagnostics for the model described by equation (1). Coefficient of determination (right), RMS error (center), and number of valid data points on which the regression at each grid box was trained (left) are shown for OMI-retrieved tropospheric column NO_2 (top) and MODIS-retrieved aerosol optical depth (middle) and liquid cloud effective radius (bottom). All diagnostic values are calculated for data between January 2005 and December 2019 only.

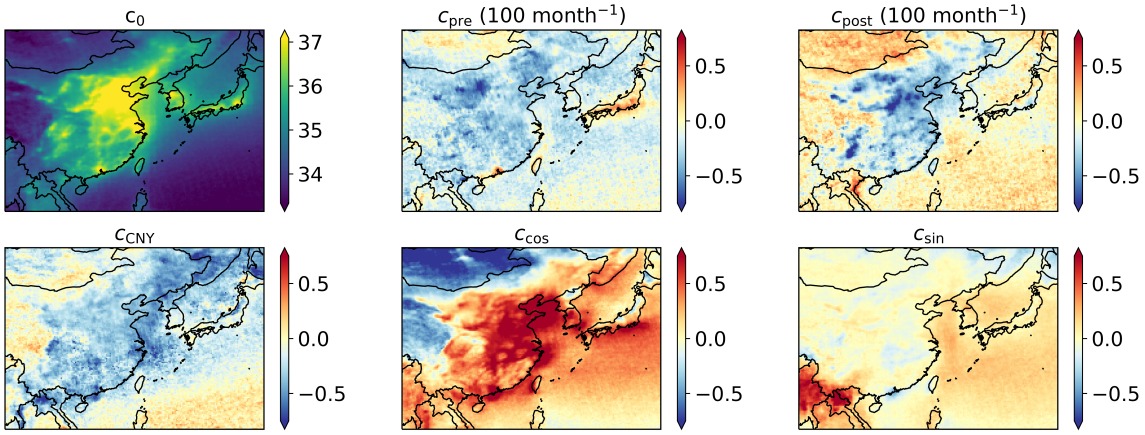

Figure S3. Maps of the regression intercept and coefficients for ln(NO_2) from OMI/Aura.

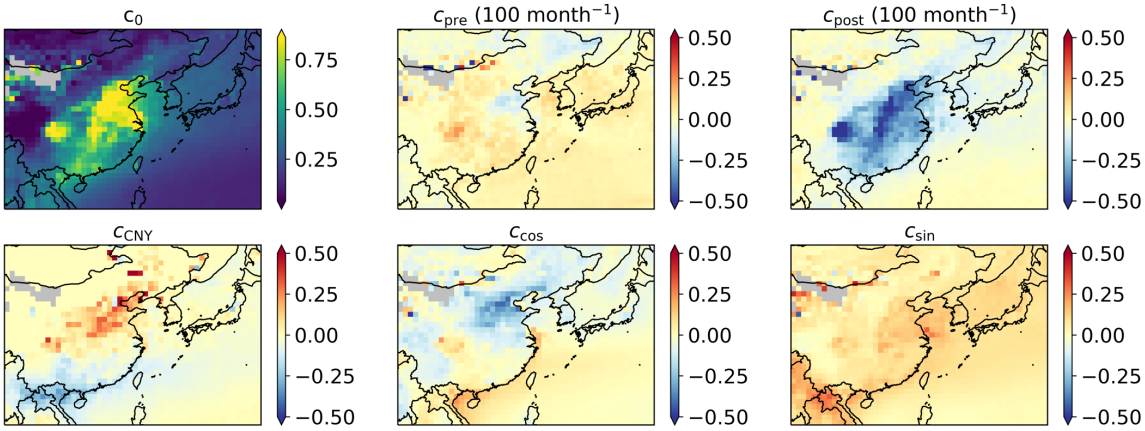

Figure S4. Maps of the regression intercept and coefficients for AOD from MODIS/Aqua.

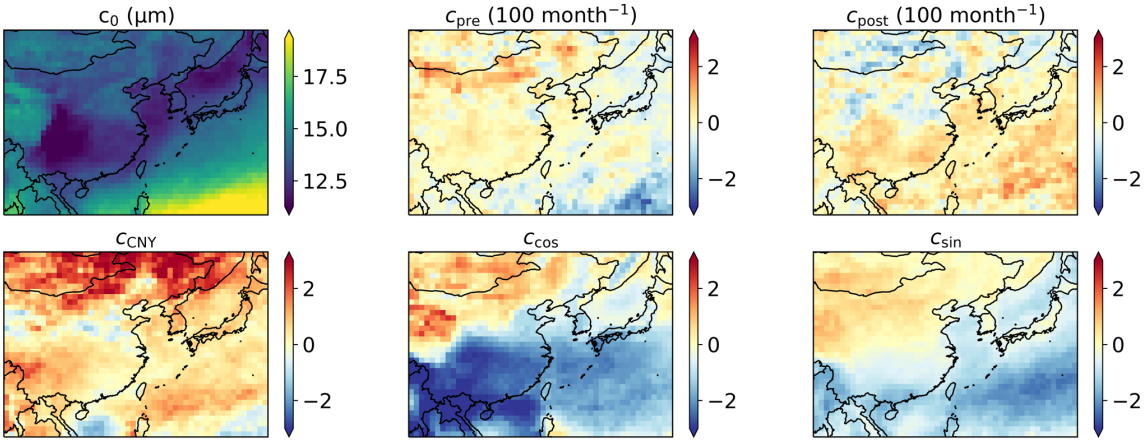

Figure S5. Maps of the regression intercept and coefficients for r_e from MODIS/Aqua.

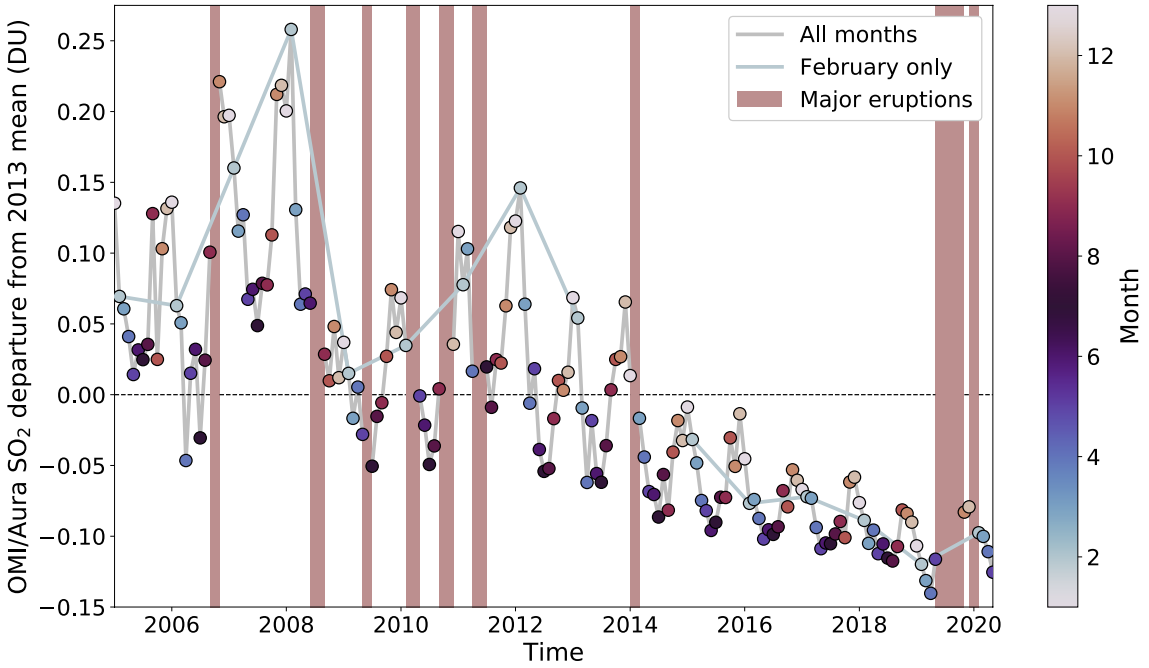

Figure S6. Time series of OMI/Aura planetary boundary layer sulfur dioxide column departures from the 2013 mean averaged over the region 20-42°N, 108-125°E (box in Figure 2ab). Marker colors refer to month and separate lines are plotted for all valid data (gray) and only data for February of each year (light blue). Data potentially affected by volcanic plumes are excluded (shading). The major Northern Hemisphere eruption events that were excluded include:

- October 2006: Rabaul, Papua New Guinea
- July 2008: Okmok, United States
- August 2008: Kasatochi, United States
- June 2009: Sarychev, Russia
- March-April 2010: Eyjafjallajökull, Iceland
- October-November 2010: Merapi, Indonesia
- May 2011: Grímsvötn, Iceland
- June 2011: Nabro, Eritrea
- February 2014: Kelud, Indonesia
- June 2019: Raikoke, Russia
- July 2019: Ulawun, Papua New Guinea
- August-October 2019: Sheveluch, Russia
- January 2020: Taal, Philippines

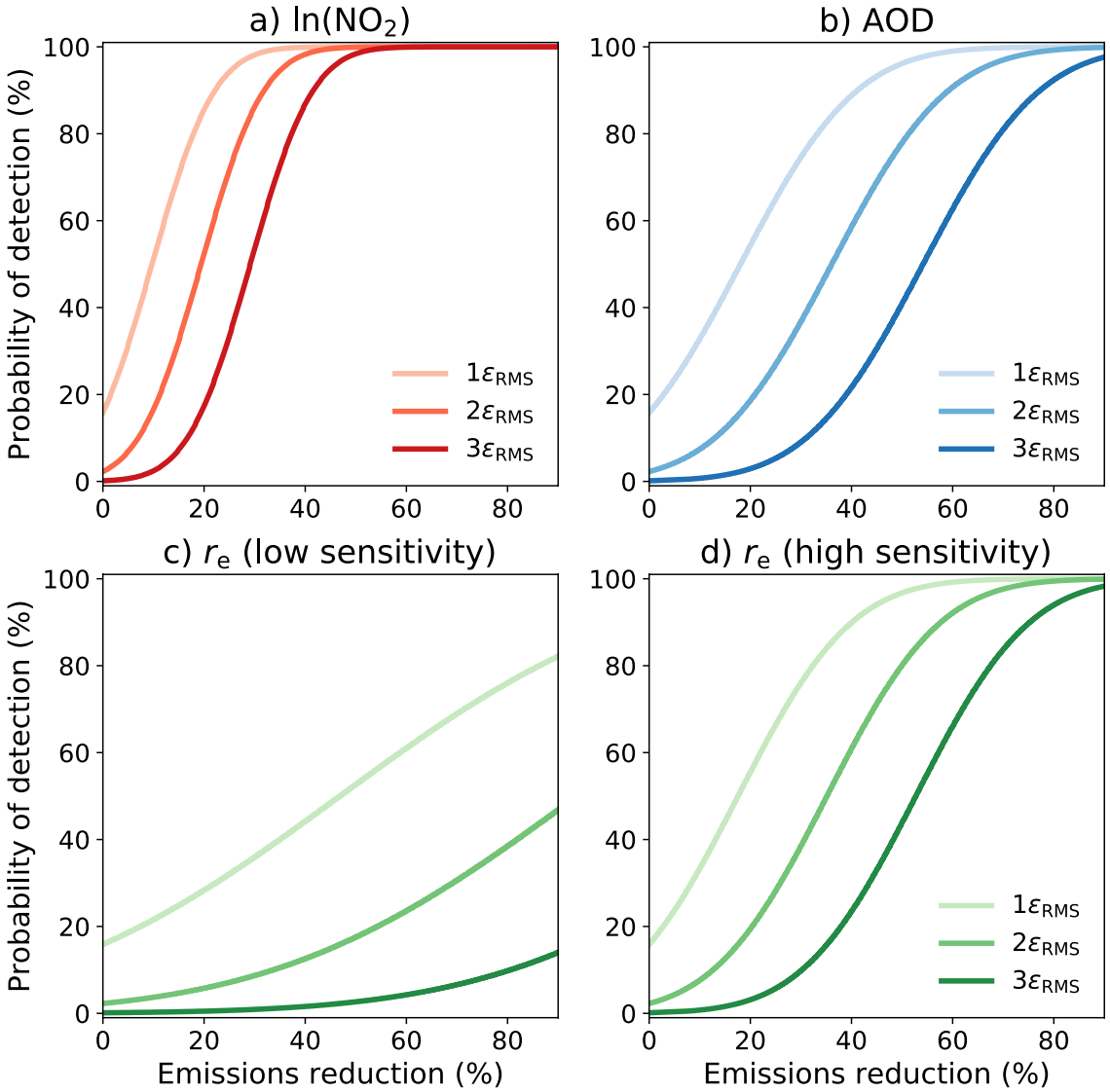

Figure S7. Probability of detecting emissions perturbations of varying sizes for **a)** ln(NO_2), **b)** AOD, and r_e assuming **c)** low ($\beta = 0.3$) or **d)** high ($\beta = 0.8$) sensitivity of cloud microphysics to aerosol, for February 2020. Light, medium, and dark lines indicate the probability of the observed value being below (NO_2, AOD) or above (r_e) one, two, and three RMS error(s) of the expected value, respectively.

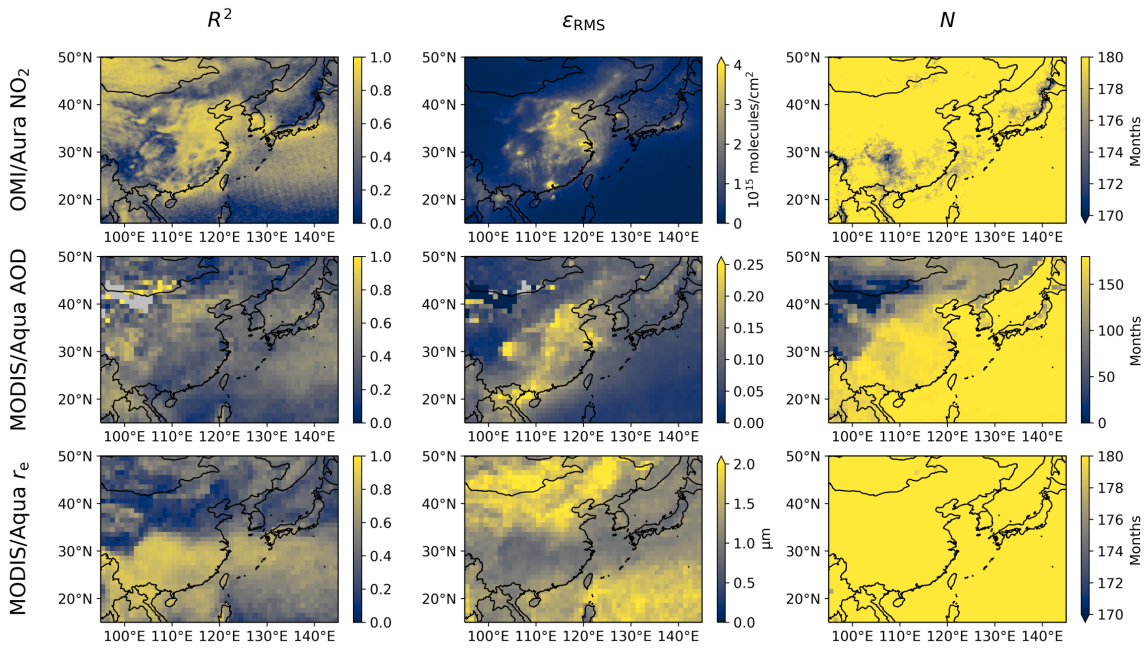

Figure S8. Maps of regression diagnostics for the model described by equation (5), including meteorological variables. Coefficient of determination (right), RMS error (center), and number of valid data points on which the regression at each grid box was trained (left) are shown for OMI-retrieved tropospheric column NO_2 (top) and MODIS-retrieved aerosol optical depth (middle) and liquid cloud effective radius (bottom). All diagnostic values are calculated for data between January 2005 and December 2019 only.

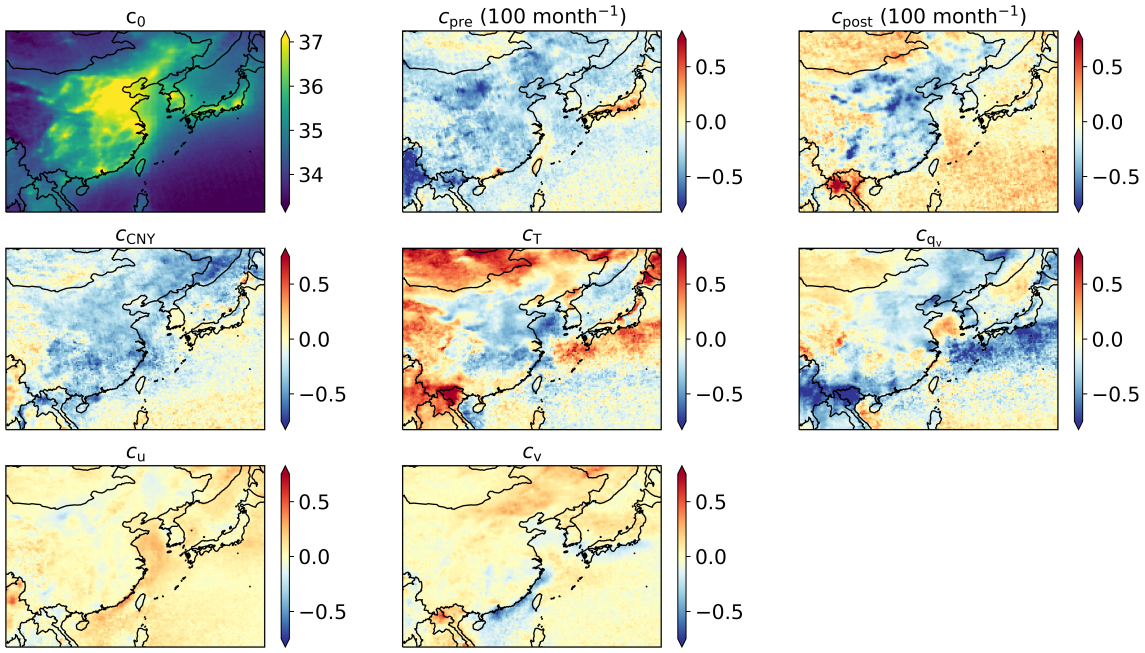

Figure S9. Maps of the regression intercept and coefficients for ln(NO_2) from OMI/Aura for the model described by equation (5).

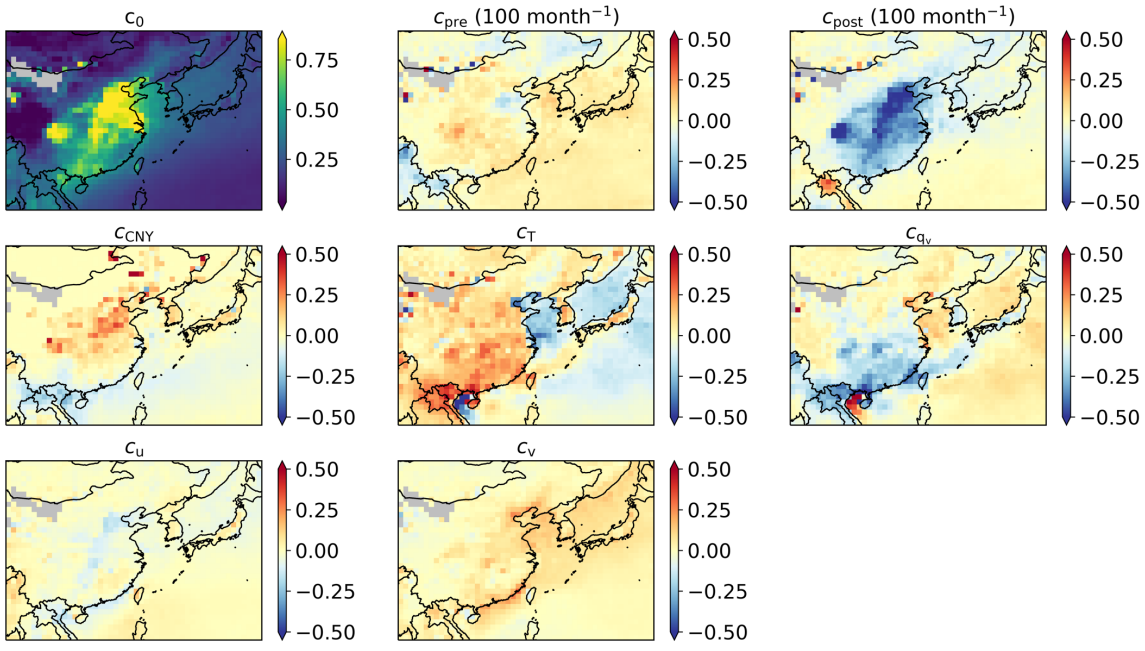

Figure S10. Maps of the regression intercept and coefficients for AOD from MODIS/Aqua for the model described by equation (5).

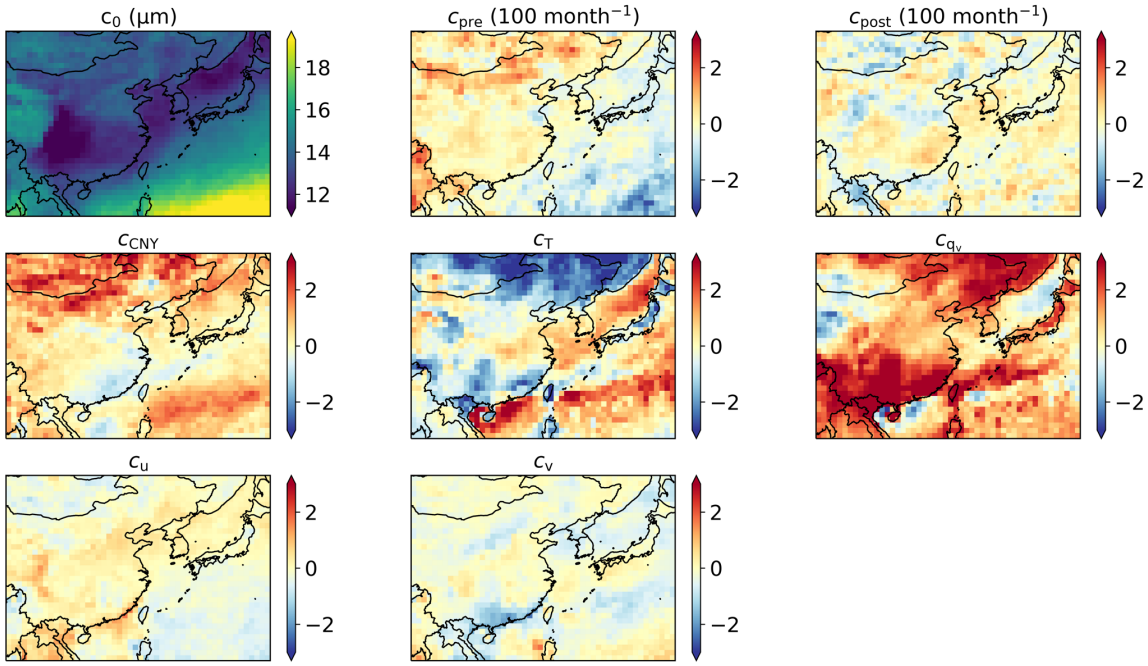

Figure S11. Maps of the regression intercept and coefficients for r_e from MODIS/Aqua for the model described by equation (5).

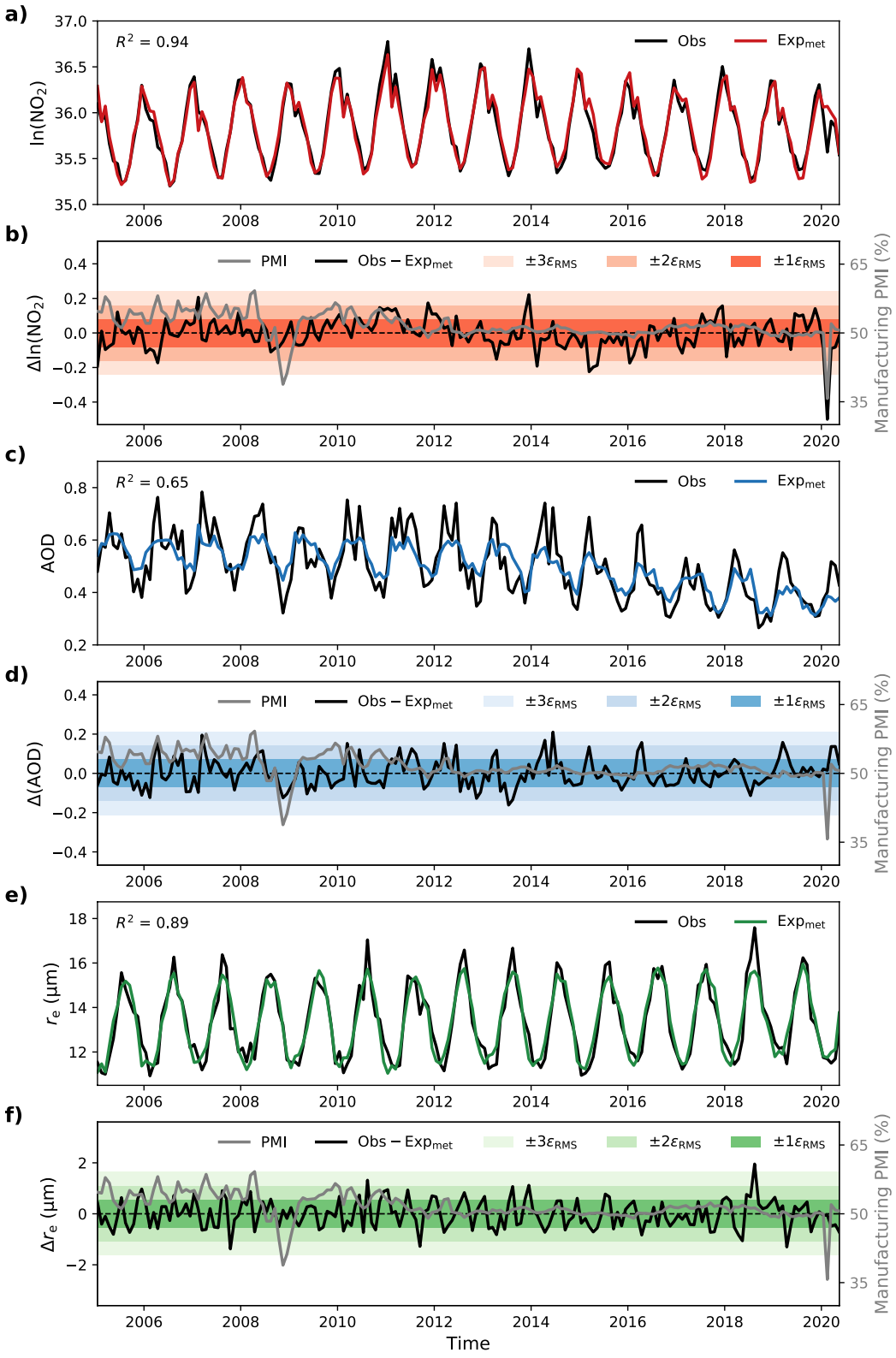

Figure S12. Time series of observed (Obs) and expected (Exp$_{met}$) values and their differences for **a-b)** ln(NO$_2$), **c-d)** AOD, and **e-f)** r_e, as averaged over the boxes in Figure 2 for the model described by equation (5). Manufacturing PMI is shown for reference.

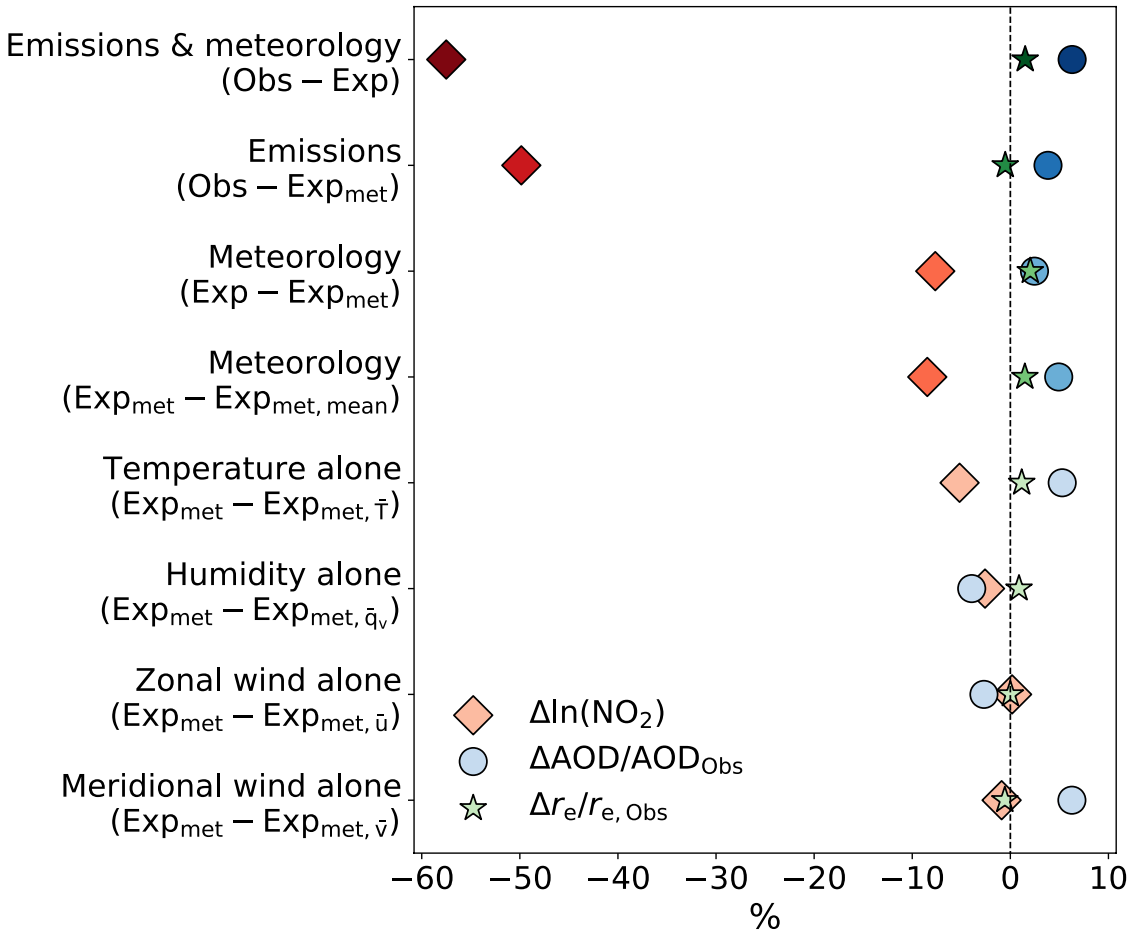

Figure S13. Decomposition of meteorology and emissions-related effects by comparing different sets of differences between the observations and linear models and their permutations for NO_2 (red diamonds), AOD (blue circles), and r_e (green stars).

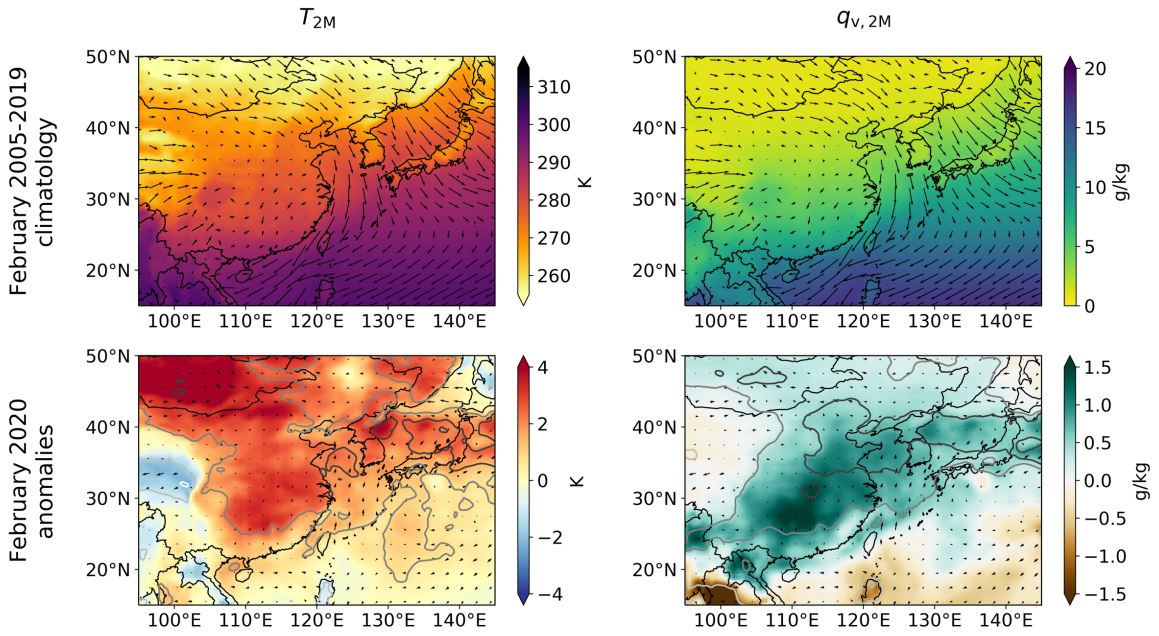

Figure S14. Maps of the February 2005-2019 climatology (top) and February 2020 anomalies (bottom) for 2-m temperature (left) and 2-m specific humidity (right). The longest wind vectors are ~10 m/s. The white to dark gray contours in the bottom row indicate anomalies exceeding -2, -1, 1, and 2 standard deviations of the 2005-2019 mean values.

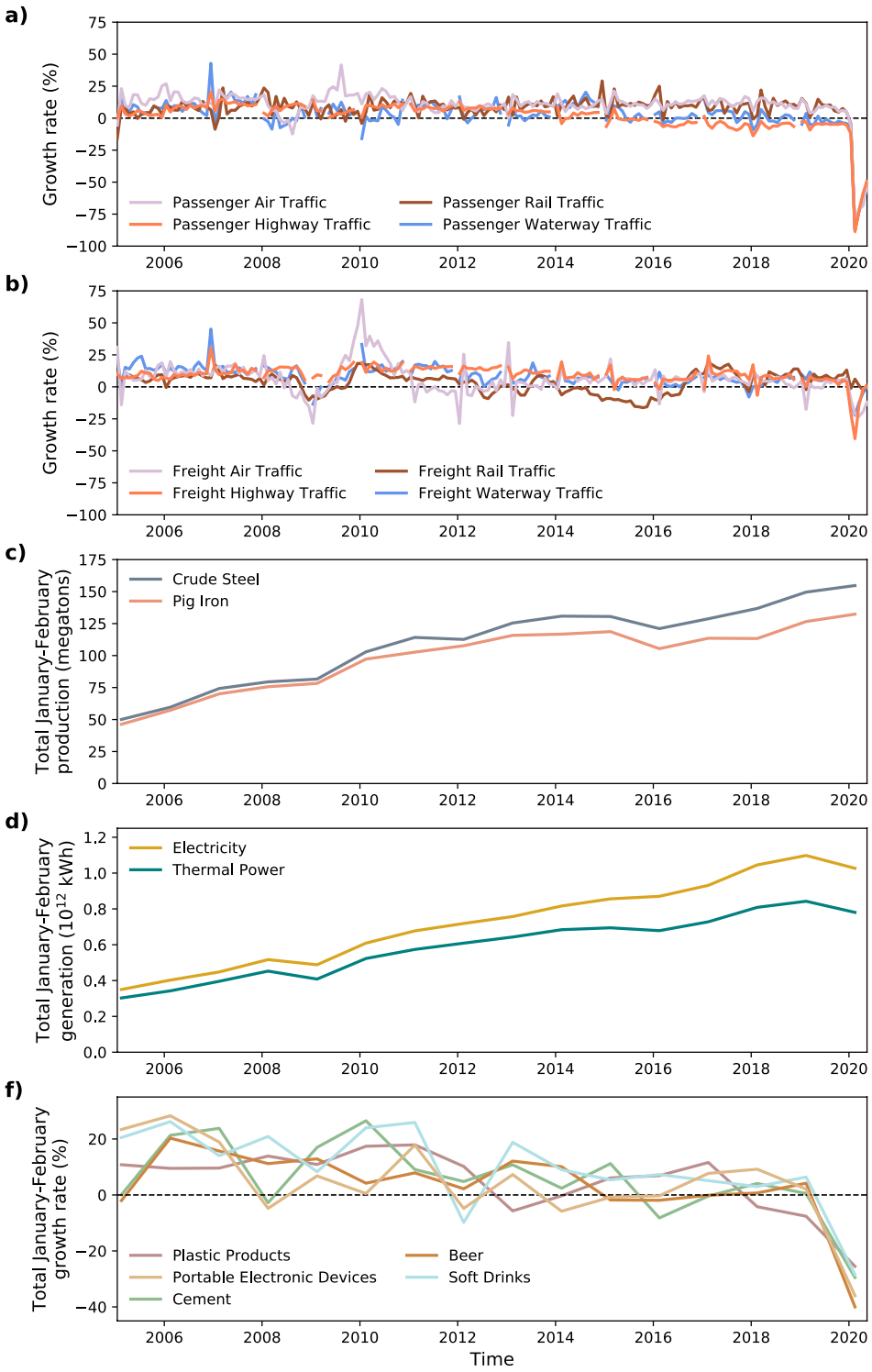

Figure S15. Timeseries of economic indicators. Changes in **a)** passenger and **b)** freight traffic are indicated by the growth rate (compared to the previous year) for each month between January 2005 and May 2020. **c)** Crude steel and pig iron production and **d)** power generation are indicated by the growth in total January-February production. **e)** Changes in various other industries as indicated by the growth rate (compared to the previous year) in total January-February production.

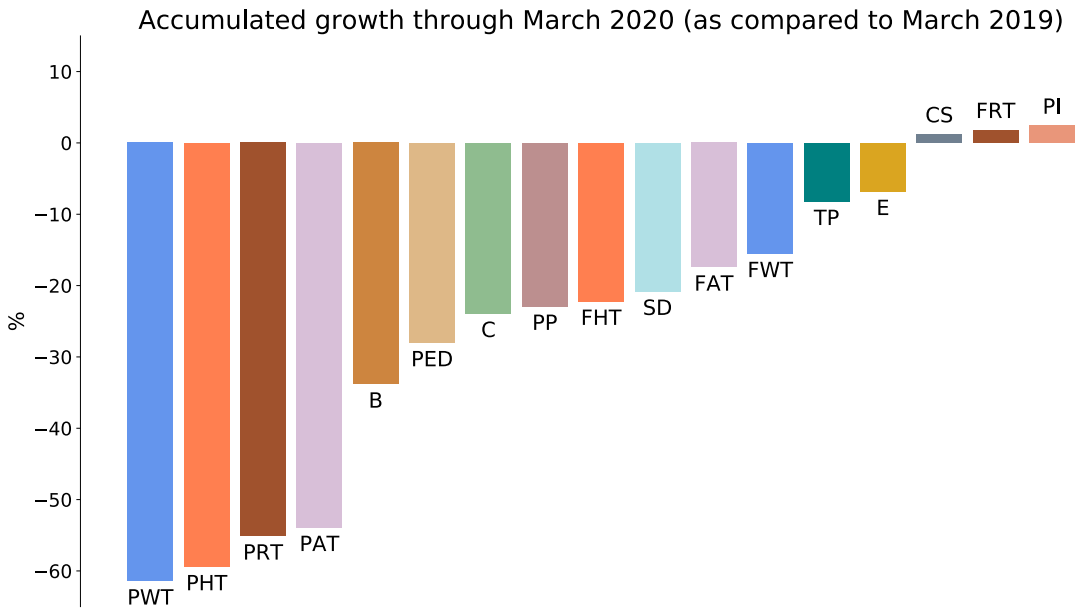

Figure S16. Comparison of the accumulated growth rate through March 2020 (i.e., total January-March production from 2020 as compared to 2019) for each economic sub-sector shown in Figure S15. Bar colors for each economic sub-sector are the same as the line colors in Figure S15. Abbreviations of the sub-sector names are as follows:

- PWT = Passenger Waterway Traffic
- PHT = Passenger Highway Traffic
- PRT = Passenger Rail Traffic
- PAT = Passenger Air Traffic
- B = Beer
- PED = Portable Electronic Devices
- C = Cement
- PP = Plastic Products
- FHT = Freight Highway Traffic
- SD = Soft Drinks
- FAT = Freight Air Traffic
- FWT = Freight Waterway Traffic
- TP = Thermal Power
- E = Electricity
- CS = Crude Steel
- FRT = Freight Rail Traffic
- PI = Pig Iron

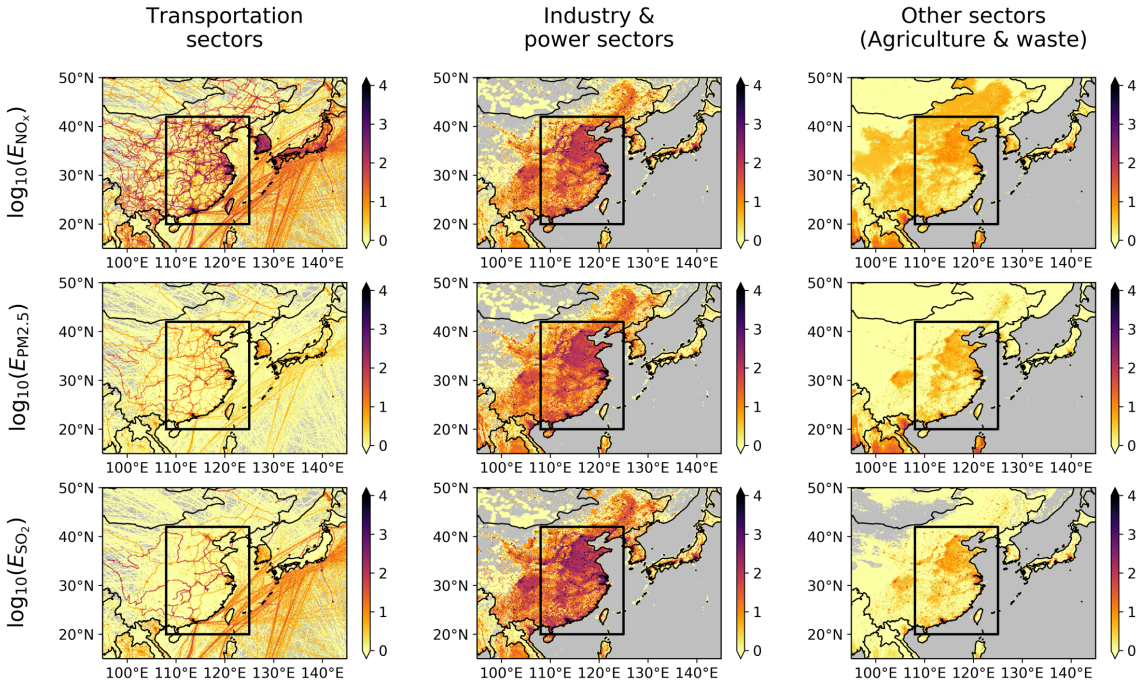

Figure S17. Emissions of major pollutants over China for 2015 from EDGAR in units of ng/m^2/s. Values for transportation (left), industry and power (center), and other sectors (right) are shown for NO_x (top), PM2.5 (middle), and SO_2 (bottom). Areas with no recorded emissions are shaded in gray. Black boxes indicate the area used in Tables S1-3. Note that shading indicates the base-ten logarithm of emissions and the scale spans five orders of magnitude.

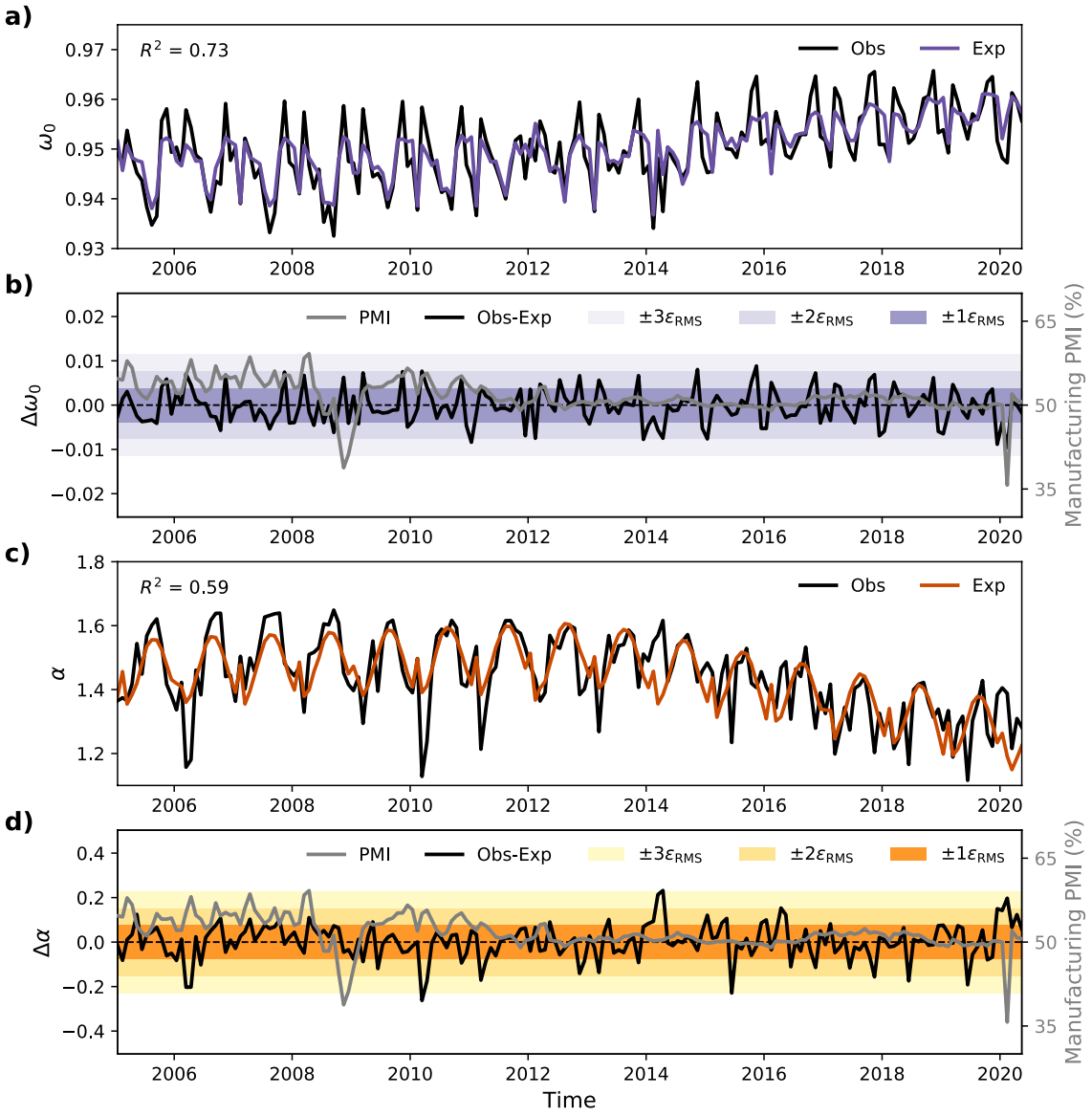

Figure 18. Time series of observed (Obs) and expected (Exp) values and their differences for **a-b)** single-scatter albedo and **c-d)** Ångström exponent, as averaged over the boxes in Figure 2. Manufacturing PMI is shown for reference.

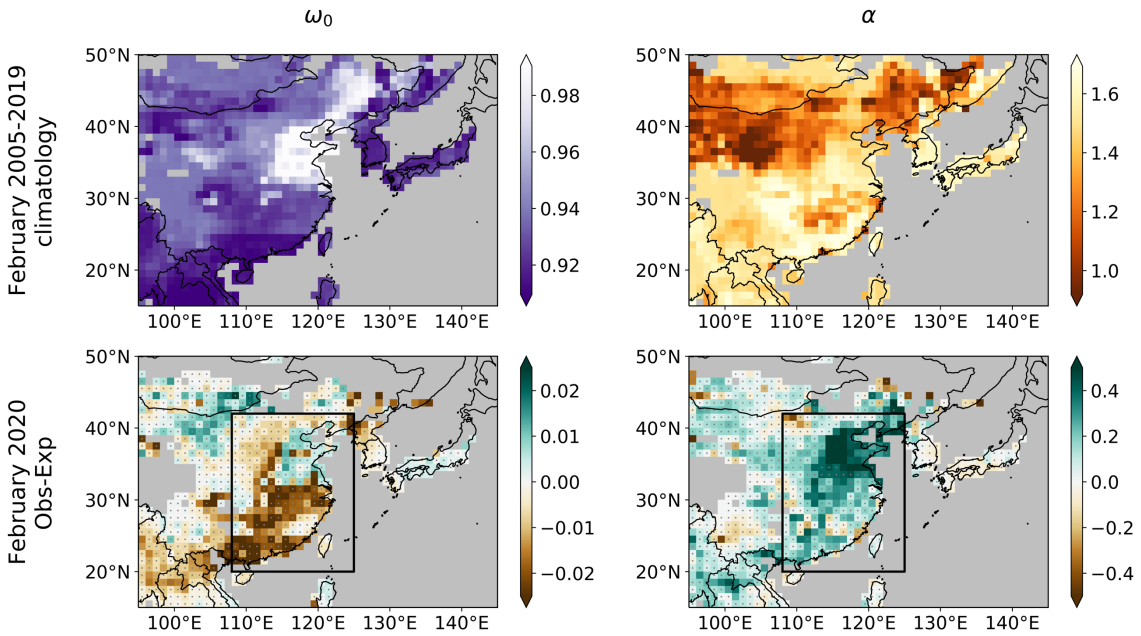

Figure 19. Maps of the February 2005-2019 climatology (top) and the difference the February 2020 observed and expected values (bottom) for the Deep Blue single-scatter albedo (left) and Ångström exponent (right). Gray stippling in the bottom row indicates absolute differences below $2\varepsilon_{RMS}$. Black boxes in the bottom row indicate areas used for the regional averages.

Transportation sectors	NO_x emissions		$PM_{2.5}$ emissions		SO_2 emissions	
(IPCC 2006 code)	Mass (Tg)	Fraction of total	Mass (Tg)	Fraction of total	Mass (Tg)	Fraction of total
Aviation climbing & descent (1A3a_CDS)	0.089	0.4%	0.002	0.0%	0.008	0.0%
Aviation cruise (1A3a_CRS)	0.102	0.5%	0.002	0.0%	0.009	0.0%
Aviation landing & takeoff (1A3a_LTO)	0.028	0.1%	0.000	0.0%	0.003	0.0%
Road transportation no resuspension (1A3b_noRES)	3.668	17.8%	0.124	1.4%	0.046	0.2%
Road transportation resuspension (1A3b_RES)	0.000	0.0%	0.030	0.3%	0.000	0.0%
Railways, pipelines, off-road transport (1A3c+1A3e)	0.225	1.1%	0.032	0.4%	0.039	0.2%
Shipping (1A3d)	1.274	6.2%	0.218	2.5%	0.829	3.2%
Transportation sub-total	**5.387**	**26.2%**	**0.407**	**4.7%**	**0.934**	**3.6%**

Table S1. Emissions from the transportation sectors over the region 20-42°N, 108-125°E for 2015 from the EDGAR emissions database. Values are reported as the total mass emitted by each sub-sector for the year and what fraction of the total emissions of each species this comprises.

Industry & power sectors	NO_x emissions		$PM_{2.5}$ emissions		SO_2 emissions	
(IPCC 2006 code)	Mass (Tg)	Fraction of total	Mass (Tg)	Fraction of total	Mass (Tg)	Fraction of total
Chemical processes (2B)	0.044	0.2%	0.028	0.3%	0.560	2.2%
Combustion for manufacturing (1A2)	7.353	35.7%	3.938	45.2%	14.428	56.3%
Energy for buildings (1A4+1A5)	0.775	3.8%	1.930	22.2%	1.582	6.2%
Fossil Fuel Fires (5B)	0.006	0.0%	0.023	0.3%	0.049	0.2%
Fuel exploitation (1B1a+1B2aiii2+1B2aiii3+1B2bi+1B2bii)	0.002	0.0%	0.001	0.0%	0.000	0.0%
Iron and steel production (2C1+2C2)	0.004	0.0%	0.160	1.8%	0.002	0.0%
Non-ferrous metals production (2C3+2C4+2C5+2C6+2C7)	0.011	0.1%	0.018	0.2%	0.171	0.7%
Non-metallic minerals production (2A)	0.000	0.0%	0.824	9.5%	0.000	0.0%
Oil refineries and Transformation industry (1A1b+1A1ci+1A1cii+1A5biii+1B1b+1B2aiii6+1B2biii3+1B1c)	0.916	4.4 %	0.869	10.0%	1.622	6.3%
Power industry (1A1a)	5.786	28.1%	0.286	3.3%	5.952	23.2%
Solvents and products use (2D3+2E+2F+2G)	0.000	0.0%	0.0	0.0%	0.000	0.0%
Industry & power sub-total	**14.897**	**72.3%**	**8.077**	**92.8%**	**24.367**	**95.1%**

Table S2. Emissions from the industry and power sectors over the region 20-42°N, 108-125°E for 2015 from the EDGAR emissions database. Values are reported as the total mass emitted by each sub-sector for the year and what fraction of the total emissions of each species this comprises.

Other sectors	NO_x emissions		$PM_{2.5}$ emissions		SO_2 emissions	
(IPCC 2006 code)	Mass (Tg)	Fraction of total	Mass (Tg)	Fraction of total	Mass (Tg)	Fraction of total
Agricultural soils (3C2+3C3+3C4+3C7)	0.223	1.1%	0.032	0.4%	0.000	0.0%
Agricultural waste burning (3C1b)	0.013	0.1%	0.028	0.3%	0.002	0.0%
Food and Paper (2H)	0.013	0.1%	0.008	0.1%	0.293	1.1%
Manure management (3A2)	0.046	0.2%	0.057	0.6%	0.000	0.0%
Solid waste incineration (4C)	0.019	0.1%	0.095	1.1%	0.018	0.1%
Solid waste landfills (4A+4B)	0.000	0.0%	0.000	0.0%	0.000	0.0%
Other sub-total	**0.314**	**1.5%**	**0.219**	**2.5%**	**0.313**	**1.2%**

Table S3. Emissions from other sectors not included above—mainly agriculture and waste management—over the region 20-42°N, 108-125°E for 2015 from the EDGAR emissions database. Values are reported as the total mass emitted by each sub-sector for the year and what fraction of the total emissions of each species this comprises.